Lyle, M., Koizumi, I., Richter, C., and Moore, T.C., Jr. (Eds.), 2000
Proceedings of the Ocean Drilling Program, Scientific Results, Vol. 167

23. GEOCHEMICAL CHARACTER OF GLACIAL TO INTERGLACIAL SEDIMENTS AT SITE 1017, SOUTHERN CALIFORNIAN MARGIN: MINOR AND TRACE ELEMENTS[1]

Tomohisa Irino[2] and Thomas F. Pedersen[3]

ABSTRACT

We analyzed selected minor and trace element contents to examine the sources and transport paths of sediments deposited at Ocean Drilling Program Site 1017 during the last 25 k.y. Elements are subsequently classified as being of diagenetic, biogenic, and/or terrigenous origins. Re, U, Mo, and As are diagenetically enriched within sediments, reflecting millennial-scale variability in bottom-water oxygenation and/or the sedimentary redox boundary depth. Sr variation is largely controlled by the input of biogenic carbonate. Using Q-mode factor analysis, variations in the 12 elements of detrital origin that remain can be explained by three factors (end-members) attributable to sand- and silt-sized detritus (Factor 2), and fine fractions with mafic (Factor 3) and felsic (Factor 1) characteristics. Elimination of the influence of grain size, temporal variations in the relative contribution from mafic materials shows that more detritus from the mafic Franciscan Complex was transported to the site during marine isotope Stage 2 than during the Holocene. This was probably due to enhanced southward littoral transport of detritus along the California margin during the latest Pleistocene.

INTRODUCTION

Ocean Drilling Program (ODP) Site 1017 on the southern California margin is ideally located to shed light on questions relating to interactions between the ocean and both high- and low-frequency climate changes. The site sits at 960 m water depth on the continental slope off Point Conception (Fig. 1) near the bottom of the modern oxygen minimum zone. Surface waters in the region are characterized by high primary and export production, a result of upwelling in the California Current system, and the area is located within the modern transition between the subarctic and subtropical zooplankton faunal zones. The chemical composition of sediments at Site 1017 is expected to be sensitive to variations in the provenance of terrigenous detritus and transport paths, both of which could be affected by changes in the California Current and/or terrestrial climate. Thus, sediments at this location can be expected to contain high-resolution records of changes in the intensity of the oxygen minimum zone, the intensity of surface circulation (Lyle, Koizumi, Richter, et al., 1997), ecological responses to climate shifts, and variability in detrital input through time.

Site 1017 also offers the prospect of adding to our understanding of global climatic teleconnections. Recent results from the analyses of cores in the Southern California Borderland Basins imply that high-frequency variability in intermediate-water renewal (Behl and Kennett, 1996) and sea-surface temperature (Mortyn et al., 1996) correlate very closely with Dansgaard-Oeschger cycles (Dansgaard et al., 1993) in central Greenland. To establish whether such millennial-scale climatic changes are manifested throughout the North Pacific or whether they are limited to the enclosed Southern California Borderland Basins, it is necessary to examine open-ocean, high-sedimentation–rate sites along the California margin, such as Site 1017.

Trace and minor element compositional information can provide a way to deduce changes in bottom-water oxygen level (Calvert and Pedersen, 1993), the sedimentary redox boundary depth (Crusius et al., 1996), and the history of biogenic deposition, all of which relate to the histories of upwelling, export productivity, and intermediate-water renewal. To set the stage for future exploration of such phenomena, we used a high-resolution suite of trace and minor element concentration data primarily to distinguish the relative contributions

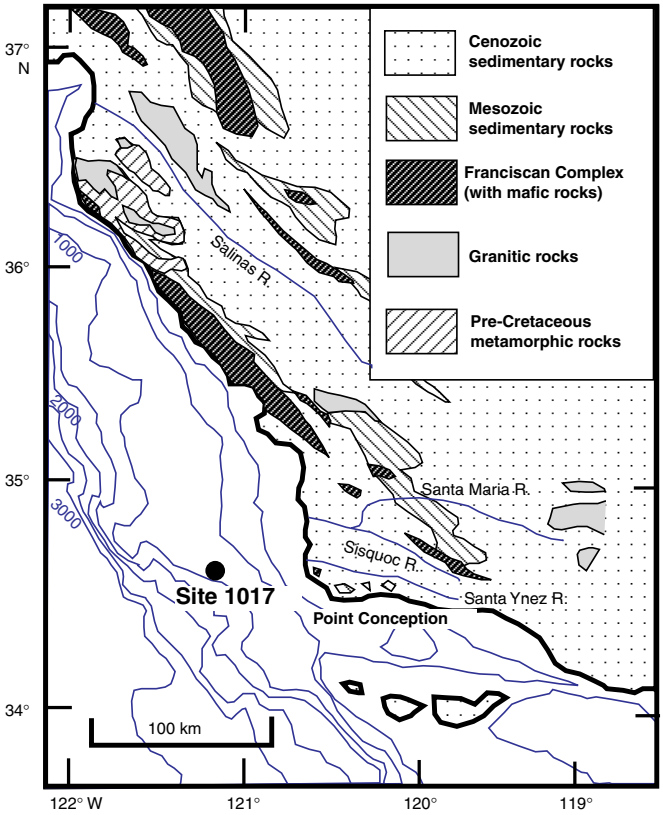

Figure 1. Location map for ODP Leg 167, Site 1017. The generalized distribution of major geological units is indicated.

[1]Lyle, M., Koizumi, I., Richter, C., and Moore, T.C., Jr. (Eds.), 2000. *Proc. ODP, Sci. Results,* 167: College Station TX (Ocean Drilling Program).

[2]Department of Earth and Planetary Sciences, Hokkaido University, Kita-10, Nishi-8, Kita-ku, Sapporo, 060-0810, Japan. (Present address: Marine Geology Department, Geological Survey of Japan,1-1-3 Higashi, Tsukuba, 305-8567, Japan. irino@gsj.go.jp)

[3]Oceanography, Earth and Ocean Sciences, University of British Columbia, 6270 University Boulevard, Vancouver, B.C. V6T 1Z4, Canada.

of diagenetic, biogenic, and detrital inputs and to establish the provenance of terrigenous detritus (Cullers, 1994). This is a necessary first step upon which subsequent paleoceanographic reconstructions will be based.

SAMPLING AND MATERIALS

Cores 167-1017E-1H through 3H were taken down to 24.9 m below seafloor (mbsf), with 103.3% recovery at Site 1017 (34°32.099′N, 121°6.430′W, 955.5 m water depth) using the advanced piston coring system (Lyle, Koizumi, Richter, et al., 1997). Results from only the upper 6 m of the section are reported here. The deposits consist mainly of calcareous silt or clay. Frequent sand patches and layers are intercalated below 250 centimeters below seafloor (cmbsf), and most show graded bedding. Sediments are moderately to heavily bioturbated and rarely show recognizable stratification such as laminations. The biosiliceous component is very small (Lyle, Koizumi, Richter, et al., 1997), and carbonate and organic carbon contents range from 0.1% to 1.5% and 0.5% to 3%, respectively (Tada et al., Chap. 25, this volume). Thus, the sediments consist of ~80%–90% inorganic detritus.

The recovered core was sealed and refrigerated on board immediately after recovery. Sampling was performed at Texas A&M University (TAMU) three months after the cruise. Hole 1017E cores were split and sampled every 3 cm from top to bottom, and then every sample was vacuum packed and stored refrigerated at TAMU. Here we use 197 samples of Core 167-1017E-1H extending from 0 to 590 cmbsf. To compare measured element profiles directly with lithostratigraphic observations based on visual descriptions of the cut surface of the core and X-ray radiography (Tada et al., Chap. 25, this volume), we use sample depth uncorrected for core expansion. This interval corresponds to 0–25 ka based on the accelerator mass spectrometry (AMS) ^{14}C dates of mixed planktonic foraminifers (Kennett et al., Chap. 21, this volume) and the boundary between marine isotope Stages (MIS) 1 and 2 located at 325 cmbsf. Bulk-sediment samples were prepared for analysis by freeze drying and were homogenized by grinding in a tungsten carbide disc mill.

METHODS

Chlorinity Analysis

Salt content (% Cl) was determined volumetrically by Knudsen-type titration (Strickland and Parsons, 1972) using $AgNO_3$ solution with K_2CrO_4 color indicator. The 1σ relative standard deviation was 3%.

Minor Element Analysis

Concentrations of V, Cr, Mn, Co, Ni, Cu, Zn, As, Rb, Sr, Y, Zr, Nb, Ba, Pb, and Ti were determined using a Phillips PW2400 X-ray spectrometer equipped with a Rh tube powered at 3 kW following the method of Calvert et al. (1985). Precisions (1σ relative standard deviations) were 30%–50% for Co, As, and Pb (all of which had low concentrations), 15% for Ni, 7% for Nb, 6% for Ba, and less than 5% for the other elements.

Trace Element Analysis

Contents of Re, Mo, and U were analyzed by isotope dilution flow-injection-analysis ICP-MS on a Plasmaquad II+ in the peak-jumping mode following the method of Crusius et al. (1996). Samples were analyzed for Re after complete microwave digestion in concentrated HCl, HNO_3, and HF, and anion exchange preconcentration using Dowex AG 1X-8 (100–200 mesh). Subsamples for Mo and U analysis were collected from a weighed fraction of the Re digest for measurement. Precisions (1σ relative standard deviation) are ~2% for Re and 5% for Mo and U.

Other Data

Organic (C_{org}) and carbonate carbon (C_{carb}) contents (analyzed by a LECO WR-12 carbon determinator), pyrite abundance (determined semiquantitatively by X-ray diffraction analysis), and volume percentages (vol%) of the silt-size component (determined by laser diffraction–scattering method) were determined by Tada et al. (Chap. 25, this volume). Depth profiles for these parameters are compared here with those for minor and trace element concentrations to examine relationships among the variations in minor and trace metals and those in biogenic, diagenetic, and detrital materials.

Corrections for Dilution by Salt

When reporting elemental concentrations in marine sediments, salt interferes both as a direct diluent and as a contributor of specific elements to the sediments. To correct for this, two assumptions were made: first, that interstitial water salinity was 35‰, and second, that the chlorine in the sediment is present entirely as salt and not within any other components. Factors for salt correction were calculated using the composition of seawater tabulated by Horne (1969). The correction for Sr was applied first, using the following equation:

$$(\text{ppm Sr})_{\text{sed}} = (\text{ppm Sr})_{\text{sed + salt}} - 4.13 \times (\%\ \text{Cl}) .$$

Specific salt corrections for other elements were not necessary because of their low concentrations in sea salt. All elemental concentrations were subsequently corrected for bulk dilution by salt using the equation

$$(\text{ppm Element})_{\text{salt free}} = (\text{ppm Element})_{\text{sed}} \times \frac{100}{100 - 1.82 \times (\%\ \text{Cl})} .$$

RESULTS

Analytical results for salt (% Cl), and salt-corrected minor and trace element concentrations are listed in Table 1. To clarify the origin of each element, the enrichment factors relative to "average crust" (Taylor and McLennan, 1985; Fig. 2) and the relationships between element depth profiles and lithofacies (Figs. 3–5) are examined. Enrichment factor is defined as

$$(\text{Enrichment factor}) = \frac{(\text{Element}/\text{Ti})_{\text{sample}}}{(\text{Element}/\text{Ti})_{\text{crust}}} .$$

Re, U, Mo, and As

Re and U are highly and moderately enriched, respectively, relative to "average crust" (Fig. 2). Concentrations vary by up to a factor of 7 over the sampled section, with the highest values occurring between 40 and 170 cmbsf and 220 and 240 cmbsf during MIS 1, and between 340 and 390 cmbsf during MIS 2 (Fig. 3A). The U distribution is similar to that of Re, and concentrations vary by up to a factor of 3 (Fig. 3A). Mo and As are moderately and highly enriched, respectively (Fig. 2). Mo maxima occur between 150 and 300 cmbsf during MIS 1, and at 390, 450, and 500 cmbsf during MIS 2. Concentrations vary by as much as a factor of 8 (Fig. 3B). Arsenic shows a similar fluctuation, missing only the distinct maximum at 150 cmbsf (Fig. 3B), which is more closely related to fluctuations in pyrite abundance (Fig. 3C; Tada et al., Chap. 25, this volume), and values vary by up to a factor of 7. Profiles of all four of these elements tend to show maxima where C_{carb} and/or C_{org} (Tada et al., Chap. 25, this volume) are relatively enriched (Fig. 3C, D).

Table 1. Salt (as Cl%) and minor and trace element concentration data, Hole 1017E.

Core, section	Interval (cm)	Depth (cmbsf)	Cl (%)	V (ppm)	Cr (ppm)	Mn (ppm)	Co (ppm)	Ni (ppm)	Cu (ppm)	Zn (ppm)	As (ppm)	Rb (ppm)	Sr (ppm)	Y (ppm)	Zr (ppm)	Nb (ppm)	Ba (ppm)	Pb (ppm)	Ti (ppm)	Re (ppb)	Mo (ppm)	U (ppm)
1H-1	0-3	1.5	2.75	129.1	141.6	306.9	9.5	57.7	28.6	109.9	4.7	125.8	295.2	22.5	170.0	13.6	693.1	15.2	4150	10.74	2.55	3.23
1H-1	3-6	4.5	3.49																	15.64	1.62	3.05
1H-1	6-9	7.5	2.92	127.1	144.6	320.8	10.2	55.2	29.2	108.6	4.9	129.6	300.3	24.4	179.2	13.8	716.7	11.2	4175			
1H-1	9-12	10.5	2.64	128.9	142.0	309.2	4.7	55.3	29.5	103.9	6.0	125.0	294.7	24.4	186.6	13.4	703.9	14.5	4103	16.80	1.48	2.84
1H-1	12-15	13.5	2.48	134.6	157.7	346.3	6.7	55.2	31.8	107.0	4.5	126.1	300.3	23.6	187.9	11.6	716.2	11.5	4089	15.90	1.39	3.13
1H-1	15-18	16.5	2.40	120.2	147.1	311.6	9.5	53.5	27.6	103.1	6.4	123.9	302.5	22.2	181.8	11.7	692.8	10.2	4035	14.69	1.80	3.22
1H-1	18-21	19.5	2.15	131.2	148.7	332.1	9.8	53.3	28.7	102.9	4.4	121.6	304.5	24.8	177.4	12.0	752.6	14.7	4124	15.88	1.61	3.00
1H-1	21-24	22.5	2.26	131.5	148.2	328.8	7.3	54.9	27.1	105.0	3.1	122.3	302.0	24.8	187.2	14.5	695.3	14.2	4131	18.46	1.52	3.40
1H-1	24-27	25.5	2.17	127.3	155.7	347.5	6.9	53.2	31.2	105.5	6.2	124.0	301.7	24.7	178.5	11.1	776.4	9.9	4175		1.44	3.53
1H-1	27-30	28.5	2.23	137.2	146.3	331.3	11.7	56.4	33.4	106.9	4.5	123.4	306.1	25.7	188.4	12.7	703.7	11.9	4143		1.41	3.29

Notes: All minor and trace element concentration data have been corrected for dilution by salt. The sample depths (cmbsf) have not been corrected for core expansion.

This is a sample of the table that appears on the volume CD-ROM.

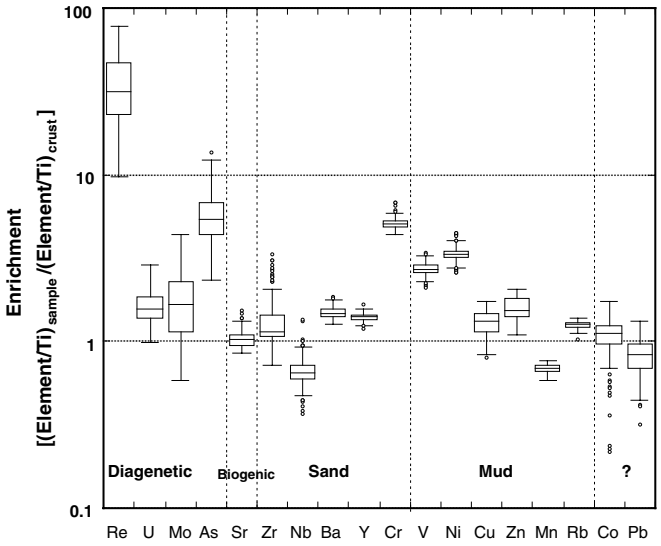

Figure 2. Box plots of relative enrichments of elements compared to "average crust" (Taylor and McLennan, 1985). The definition of enrichment factor is described in the text. Sources or textural associations of the elements as inferred from their depth profiles are also shown.

Sr

The depth profile of Sr resembles that of C_{carb} (Fig. 3D). Although the element is not significantly enriched relative to average crust (Fig. 2), it does exhibit a clear maximum of ~400 ppm at 220 cmbsf (Fig. 3D). The Sr content varies by a factor of only 1.5 over the course of the section.

Zr, Nb, Ba, Y, and Cr

Zr, Nb, Ba, Y, and Cr are equal to or are enriched relative to "average crust" (Fig. 2). All sand patches and layers are associated with the maxima of some or all of these elements (Fig. 4). These elements also show minima at 220 cmbsf where carbonate carbon shows a maximum (Tada et al., Chap. 25, this volume). Zr and Nb contents vary downcore by a maximum factor of 4, whereas Ba, Y, and Cr vary by up to a factor of 1.5. The average concentration of Cr during MIS 1 is slightly lower than that during MIS 2.

V, Ni, Cu, Zn, Mn, Rb, and Ti

V, Ni, Cu, and Zn are enriched relative to "average crust" (Fig. 2). Concentration minima occur in sand patches and layers, and concentrations overall vary over a two-fold range (Fig. 5A, B). Average contents of V and Ni during MIS 1 are approximately the same as those during MIS 2, whereas average levels of Cu and Zn during MIS 1 are higher than those during MIS 2. Mn and Rb are slightly depleted and enriched, respectively, relative to "average crust" (Fig. 2). Mn, Rb, and Ti also show minimum concentrations within sand patches and layers (Fig. 5C, D). The average Mn content during MIS 1 is lower than that during MIS 2. Each of these seven elements shows a minimum at 220 cmbsf corresponding to the carbonate carbon maximum.

Co and Pb

Co and Pb contents are approximately equal to those in "average crust" (Fig. 2). Because the amplitudes of variations in these elements are comparable to analytical error, characteristics of their profiles are hard to describe. Thus, these elements will not be mentioned further in this report.

SOURCES OF ELEMENTS

Diagenetically Enriched Elements

It is well known that enrichments of Re, U, Mo, and As imply the depletion of O_2 in bottom water and/or shallow pore waters. However, subtle geochemical contrasts among the group allow the relative intensity of oxygen depletion to be assessed. For example, while Re and U are chemically reduced and sequestered under suboxic conditions (where O_2 is absent and nitrate reduction prevails), Mo is chemically reduced only at lower redox potentials (Calvert and Pedersen, 1993; Crusius et al., 1996), and As is concentrated in horizons of diagenetic pyritization (Thomson et al., 1998) where sulfate reduction is occurring at least locally. Thus, the resemblances between the depth profiles of Re and U and their enrichment throughout the sampled section (Fig. 3A) imply that the near-surface sediments at Site 1017 have been at least suboxic throughout the last 25 k.y. The more episodic Mo and As enrichments (Fig. 3B) reflect intervals when sulfate was being reduced in either the bottom waters or the near-surface pore waters. Further evidence for the primarily diagenetic origin of these four elements can be seen in the absence of dilution in the sandy layers, implying postdepositional addition and by the relative enrichments at 220 cmbsf where there is a C_{carb} concentration peak (Fig. 3A, B, D).

A low Mo content compared to the Re enrichment in the sediments between 220 and 240 cmbsf implies that bottom waters were suboxic during deposition. Higher Mo concentrations in the deposits at 150 and 300 cmbsf indicate stronger O_2 depletion at that time (Crusius et al., 1996). These Mo-enriched horizons are accompanied by high C_{org}, which suggests that the oxygen concentration in near-interface pore waters and bottom waters was depleted by an enhanced C_{org} settling flux. However, the lack of As and pyrite maxima at 150 cmbsf implies different processes of fixation for Mo and As. Molybdenum, for example, could be scavenged by labile organic matter still

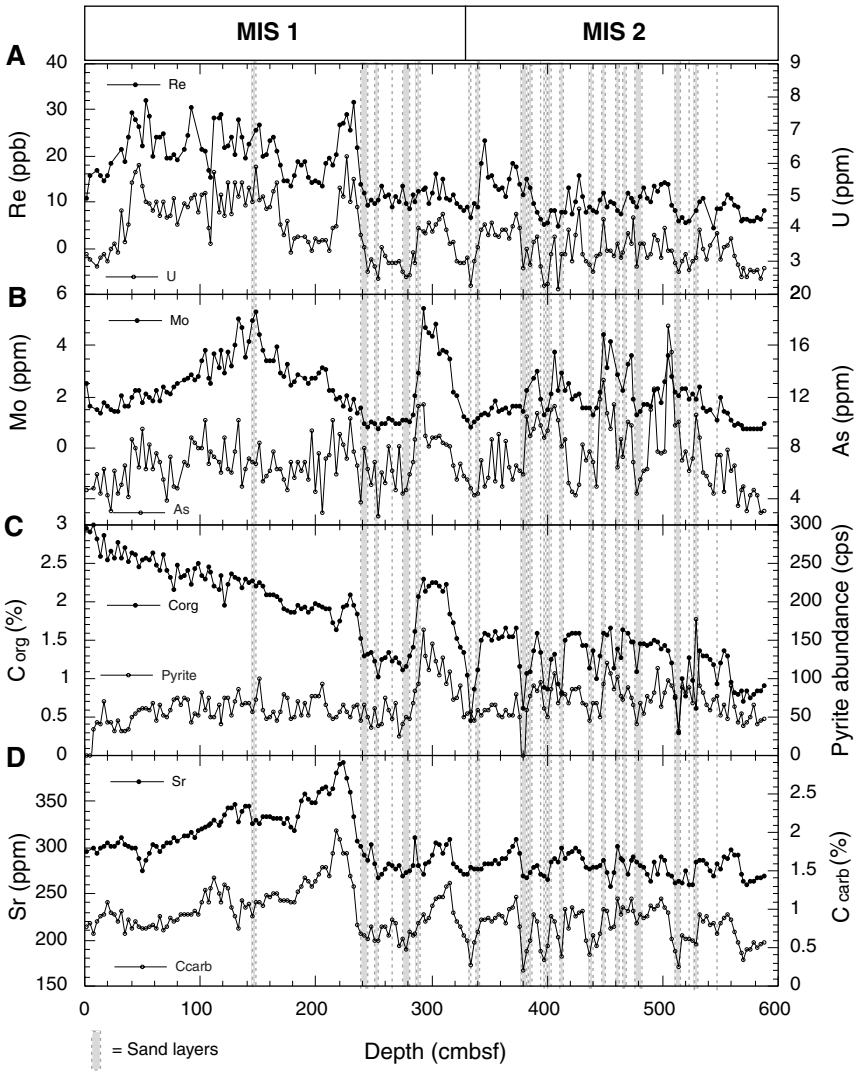

Figure 3. Depth profiles of (**A**) Re, U; (**B**) Mo, As; (**C**) organic carbon, pyrite abundance; and (**D**) Sr, carbonate carbon concentrations. Sand layers and patches based on visual core description and observation on X-ray radiographs by Tada et al. (Chap. 25, this volume) are indicated by the shaded bands in the profiles. The marine isotope stage (MIS) boundary (top panel) is based on Kennett et al. (Chap. 21, this volume).

present above a "burn-down" level (Dean et al., 1997; Dean and Gardner, 1998), or it could have coprecipitated with FeS (Calvert and Pedersen, 1993) under conditions where FeS was not converted to pyrite. This could explain the lack of an arsenic concentration peak at this horizon if As enrichment specifically requires pyrite formation (Thomson et al., 1998). In MIS 2, the Mo and As distributions imply episodically low O_2 conditions that are not associated with significant C_{org} maxima. This may suggest that short-lived intervals of oxygen depletion during MIS 2 were not induced only by an enhanced C_{org} settling flux but also by remote forcing of the O_2 content of the intermediate or bottom waters at 1 km depth.

Biogenic Elements

The close interrelationship of the Sr and carbonate carbon profiles (Fig. 3D) suggests that the variation of Sr is mainly controlled by changes in the biogenic carbonate content. A 1% difference in carbonate carbon corresponds to an 80 ppm difference in Sr, which is consistent with usual Sr concentration in biogenic carbonate (Graham et al., 1982). Approximately 200 ppm of Sr might be contributed by some other (probably detrital) phase or phases.

Detrital Elements

The distributions of elements such as Zr, Nb, Ba, Y, and Cr, which are highly enriched within sand layers and sandy patches (Fig. 4), clearly seem to be controlled by the proportion of coarse-grained terrigenous detritus in the deposits. Significant Cr enrichments relative to "average crust" imply contributions from mafic and/or ultramafic source materials (Cullers, 1994). In contrast, elements depleted within sand layers and patches such as V, Ni, Cu, Zn, Mn, Rb, and Ti seem to be contributed primarily by the fine-grained terrigenous fraction (Fig. 5A, B). Dean et al. (1997) pointed out the possibility that excess (over detrital) concentrations of Cu, Ni, and Zn were associated with an organic fraction based on interrelationships among element concentrations in Core F2-92-P29 collected from off southern California. However, the detrital fraction at Site 1017 is approximately twice as large as that at Core F2-92-P29, whereas the biogenic fraction at Site 1017 is half of that at Core F2-92-P29. Furthermore, concentrations of V, Ni, Cu, and Zn in Site 1017 sediments are much higher than expected based on the C_{org} content and consideration of the minor element contents in marine plankton (Piper, 1994). Thus, the concentrations and amplitudes of variations of these elements do not seem to be explained by contributions from the organic fraction. The enrichments of Cu, Ni, and Zn as well as V relative to "average crust" at Site 1017 could instead be explained by the contributions from mafic and/or ultramafic terrigenous materials (Cullers, 1994; Matsuo, 1989). Smaller amplitudes of fluctuation of Mn, Rb, and Ti (Fig. 5C, D) compared to V, Ni, Cu, and Zn (Fig. 5A, B) suggest that the former occur in both the fine and coarse fractions. Differences in the average concentrations of Cu, Zn, and Mn between MIS 1 and 2 suggest that the chemical composition of the fine fraction changed in

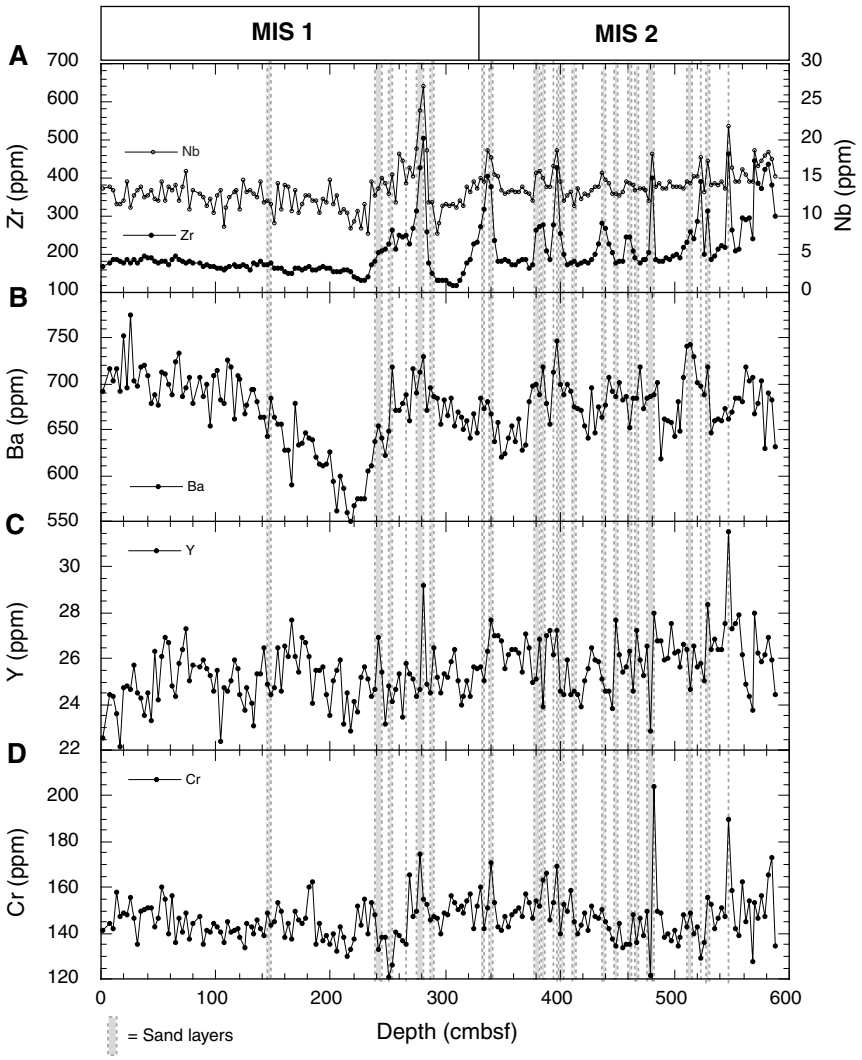

Figure 4. Depth profiles of (**A**) Zr, Nb; (**B**) Ba; (**C**) Y; and (**D**) Cr concentrations. Sand layers and patches are indicated by the stippled bands in the profiles. Sand layers and patches based on visual core description and observation on X-ray radiographs by Tada et al. (Chap. 25, this volume) are indicated by the shaded bands in the profiles. The marine isotope stage (MIS) boundary (top panel) is based on Kennett et al. (Chap. 21, this volume).

the transition from the glacial to the interglacial. Finally, the common depletion of all 12 detrital elements at 220 cmbsf, where carbonate carbon is at a maximum, confirms their assignment to the detrital category.

Q-MODE FACTOR ANALYSIS OF DETRITAL MINOR ELEMENTS

The concentrations of Zr, Nb, Ba, Y, Cr, V, Ni, Cu, Zn, Mn, Rb, and Ti show large variations downhole (Figs. 4, 5) that are sensitive to the presence or absence of sand. There is also variability in the mud-dominated intervals in the hole, however, indicating a second control that may be related to changes in the provenance of the fine-grained fraction. To distinguish semiquantitatively the common causes (factors) for variations in the distributions of these 12 "detrital" elements, such as the changes in grain-size and provenance, we have conducted Q-mode factor analysis using the element concentration data.

Prior to the factor analysis, the total concentrations of the 12 elements were normalized to unity as follows:

$$Zr + Nb + Ba + Y + Cr + V + Ni + Cu + Zn + Mn + Rb + Ti = 1.$$

This normalization eliminates apparent fluctuations in concentration attributable to dilution by biogenic materials. It also permits us to convert the factor scores and loadings, respectively, into the original elemental compositions and the actual contribution of each factor to discrete samples (Miesch, 1976). Following the normalization, each variable (as the normalized content of each element) was then proportionally rescaled to set the maximum and minimum values to one and zero, respectively. Q-mode factor analysis with varimax rotation was performed on these rescaled data (Miesch, 1976).

The Q-mode analysis yields three factors that explain 97% of the total variance in the rescaled data, implying three common end-members within the sediments. The extracted varimax factors are denoted Factor 1 through 3 in descending order of the variance explained by each. The compositions of each end-member were calculated from its varimax factor scores (Miesch, 1976) and are shown in Table 2 as element:Ti ratios. Two types of relationships between the selected element ratios in end-members and those in the samples are also shown in Figure 6. Temporal variations in the contributions of the three end-members calculated from their factor loadings are shown in Figure 7A and 7B, where the total sum of Factors 1 to 3 is unity.

Factor 2 is characterized by higher Zr/Ti, Nb/Ti, Y/Ti, Ba/Ti, and Cr/Ti ratios (Table 2; Fig. 6). The contribution of Factor 2 is highest in samples from sandy layers or lenses (Fig. 7A). Figure 7A also shows the volume percentage (vol%) of the silt-sized component within the detrital fraction of nonsand samples. These were selected mostly from the upper 2 m of the hole to examine grain-size changes within the mud-dominated intervals (Tada et al., Chap. 25, this volume). They show that the contribution of Factor 2 varies to some de-

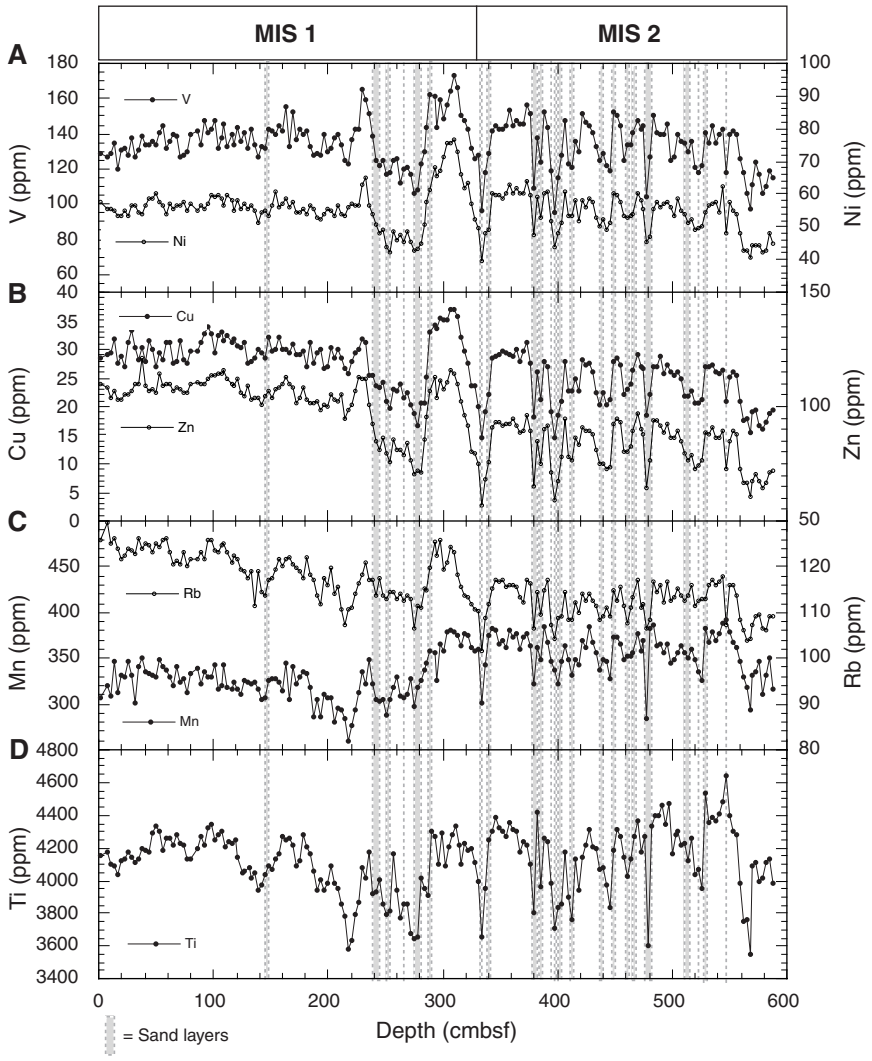

Figure 5. Depth profiles of (**A**) V, Ni; (**B**) Cu, Zn; (**C**) Mn, Rb; and (**D**) Ti concentrations. Sand layers and patches are indicated by the stippled bands in the profiles. Sand layers and patches based on visual core description and observation on X-ray radiographs by Tada et al. (Chap. 25, this volume) are indicated by the shaded bands in the profiles. The marine isotope stage (MIS) boundary (top panel) is based on Kennett et al. (Chap. 21, this volume).

Table 2. Minor element compositional ratios (relative to Ti) of each factor (detrital end member) calculated by Q-mode factor analysis.

	Factor 1 (felsic mud)	Factor 2 (sand and silt)	Factor 3 (mafic mud)
V/Ti	0.0347	0.0244	0.0478
Cr/Ti	0.0307	0.0415	0.0304
Mn/Ti	0.0559	0.0842	0.1287
Ni/Ti	0.0150	0.0092	0.0196
Cu/Ti	0.0103	0.0028	0.0074
Zn/Ti	0.0396	0.0125	0.0129
Rb/Ti	0.0353	0.0275	0.0157
Y/Ti	0.0055	0.0070	0.0055
Zr/Ti	–0.0001	0.1212	–0.0168
Nb/Ti	0.0017	0.0055	0.0012
Ba/Ti	0.1675	0.1949	0.0806

gree in harmony with the silt content (as vol%) even in the mud-dominated intervals. Thus, Factor 2 is interpreted as representing the coarser (sand and silt) portion of the detrital fraction.

The contributions of Factors 1 and 3 are lowest in samples from sandy layers or lenses (Fig. 7B). Thus, these two factors are expected to reflect the compositions of the fine fractions of terrigenous detritus from different sources. Factor 3 is distinguished from Factor 1 by its higher V/Ti, Ni/Ti, and Mn/Ti, and lower Rb/Ti, Cu/Ti, Zn/Ti, and Ba/Ti ratios (Table 2; Fig. 6). Relative enrichments of compatible elements such as V and Ni and depletion of incompatible elements such as Rb and Ba within Factor 3 imply that this factor represents contributions to the deposits from a mafic source or sources (Wilson, 1989). To examine temporal variations in relative contributions from different source rocks (essentially mafic vs. felsic) within the fine detrital fraction, the mafic contribution is defined as

$$\text{mafic contribution} = \frac{\text{Factor 3}}{\text{Factor 1} + \text{Factor 3}}.$$

The results are shown in Figure 7C. Although not perfect, this approach filters out much apparent variation that could result from dilution by the coarser fraction.

DISCUSSION

Figure 7C clearly shows that mafic contributions to the finer fraction of the detritus were higher during MIS 2 than in MIS 1. The fact that the Cr concentration in MIS 1 is lower than in MIS 2 (Fig. 4D) implies that a weakened mafic contribution also applies to the coarser fraction.

Potential sources of detrital materials for Site 1017 are (1) the Central Californian Coastal Ranges, which comprise mainly the Franciscan Complex with its associated mafic and ultra-mafic rocks; and (2) the Southern Californian Transverse Range, which mainly

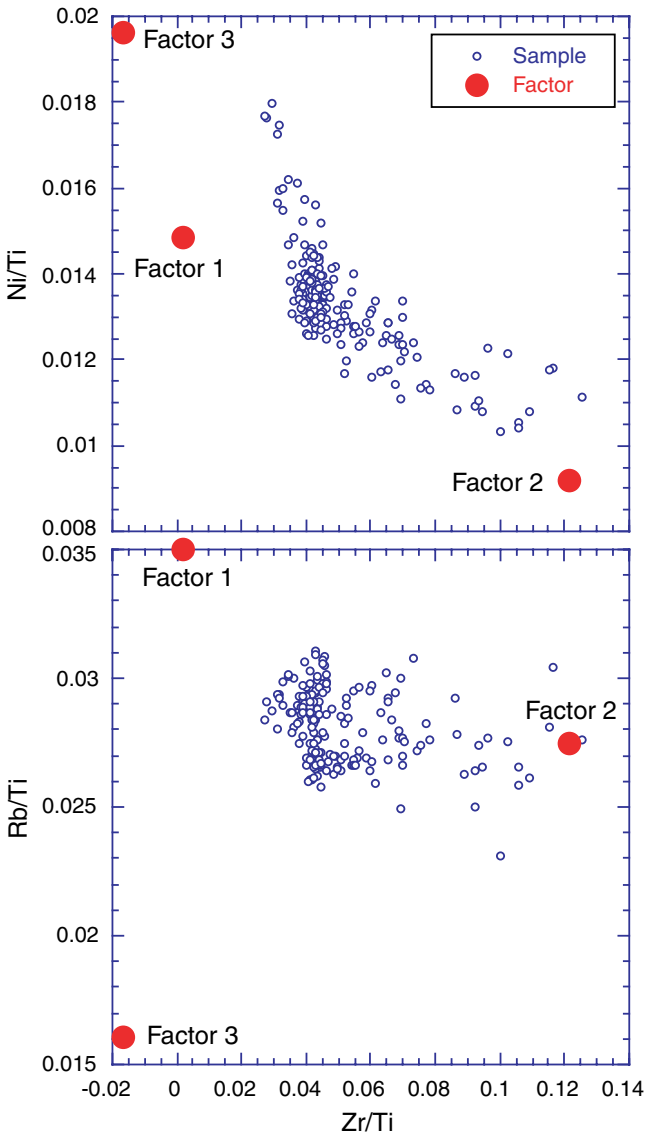

Figure 6. Interrelationships between elemental compositions of samples (shown as ratios) and those of three factors (compositional end-members of detritus) calculated by Q-mode factor analysis.

consists of Mesozoic to Cenozoic sedimentary rocks and granodiorite (Norris and Webb, 1990; Fig. 1). These basic observations imply that input of both fine and coarse detritus from Central California to Site 1017 was relatively higher during MIS 2 and lower during MIS 1.

There are three possible explanations for these variations. The first is that strengthened flow of the California Current during MIS 2 could have transported more detritus southward from a northern Franciscan source. However, previous paleoceanographic studies along the western margin of North America between Oregon and northwest Mexico suggest that the southward-flowing California Current was weaker during glacial stages (Lyle et al., 1992; Dean et al., 1997; Doose et al., 1997; Ganeshram and Pedersen, 1998) as a result of a diminished atmospheric pressure gradient between the Pacific Ocean and the ice-covered northern North American landmass (Kutzbach et al, 1993). A second potential explanation is that there was increased runoff (higher precipitation) from Central California relative to the southern region of the state during MIS 2. Based on reconstruction of lake levels, Benson et al. (1995) claimed that the southward migration of the average position of jet stream during MIS 2 enhanced precipitation in northern California. This is consistent with the observation of Gardner et al. (1997) that the terrigenous mass accumulation rate off Central California was higher during MIS 2, and their inference that precipitation in Central California was enhanced at that time. Gardner et al. (1997) also pointed out that the main detrital source could have been the Santa Maria-Sisquoc River system, which runs through the Transverse Range. However, this would have enhanced the supply of felsic materials, contrary to the observed increase in mafic input during MIS 2. Therefore, enhanced precipitation is unlikely to have provided the major control on the provenance of sediments at Site 1017. The third explanation, which fits better with our data, is that southerly littoral currents during MIS 2 transported more Franciscan-derived mafic detritus southward. In support of this, Trask (1952) showed that the heavy mineral composition of sand on modern beaches along the coast of central to southern California changes systematically from north to south. He inferred that the heavy minerals largely originated from the north and were carried toward the south in the littoral drift. Increased storminess during MIS 2 associated with the southward migration of the jet stream and associated storm tracks (Benson et al., 1995; Kutzbach et al, 1993) would have strengthened the waves that arrive at the Central Californian coast, resulting in stronger littoral drift. Furthermore, sea level was as much as 120 m lower during MIS 2 and this may have had an effect by shifting the shoreline and the zone of littoral drift to what is today the outermost shelf, that is, closer to Site 1017. We speculate that such a migration could have promoted increased deposition of mafic minerals in the area of Hole 1017E during the last glacial stage.

If our hypotheses are valid, element compositions of Site 1017 sediments have been sensitive to past migrations of the jet stream and to storm and sea-level history on the coast of central and southern California. To confirm such basic controls on the composition of terrestrial detritus in the region, the patterns of fluctuations need to be studied over a broader area and further back in time.

CONCLUSIONS

We analyzed the minor and trace element contents in a suite of 197 samples corresponding to the last 25 k.y. to examine with high resolution the provenance and upstream transport paths of sediments deposited at ODP Site 1017, as well as to define selected diagenetic enrichments. The following observations can be made:

1. Re, U, Mo, and As are diagenetically enriched within sediments, which implies perennial oxygen depletion at 1 km depth on the south-central California margin for at least the last 25 k.y.
2. The depth profiles of these elements imply that higher export production from the middle to early MIS 1 fostered severe O_2 depletion in near-interface pore waters. The relative independence of the C_{org} and Mo profiles on the millennial scale during MIS 2 suggests that intermediate-water hydrography was more important than the vertical settling flux of C_{org} in controlling the relative oxygen deficit.
3. Sr variations are largely controlled by the input of biogenic carbonate.
4. Q-mode factor analysis of a minor element assemblage associated with terrigenous detritus suggests that compositional variations are the result of a textural control (variable mixtures of sand- and silt-sized detritus) and a provenance control (variable inputs of mafic and felsic finer grained detritus).
5. Temporal variations in composition indicate that the contribution of the mafic end-member was higher during MIS 2 than during MIS 1. This can best be explained as the result of en-

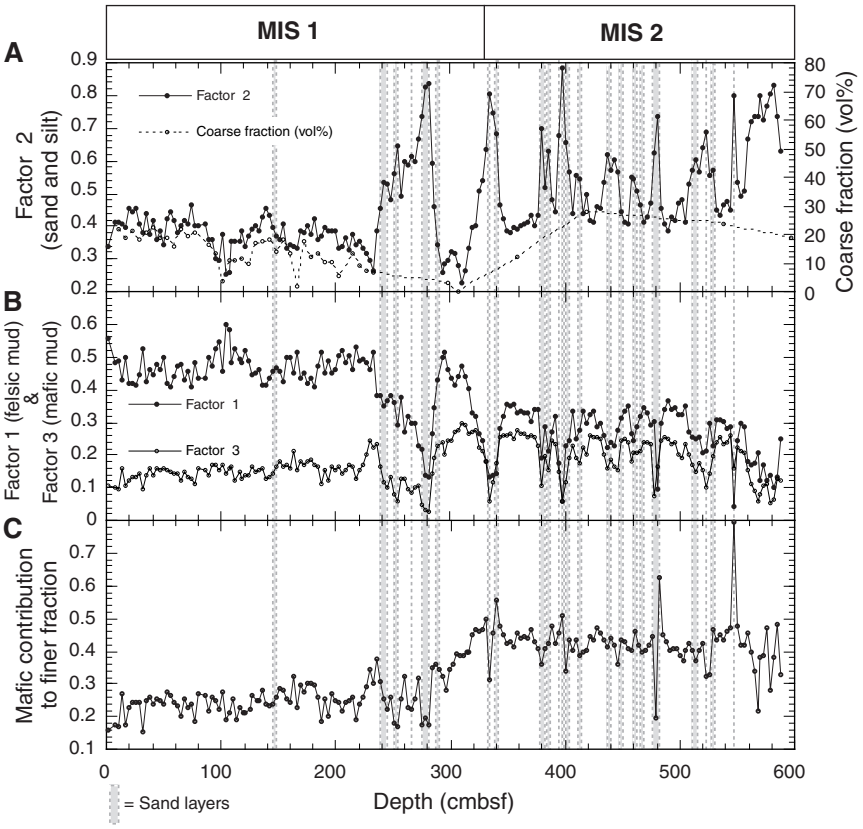

Figure 7. Depth profiles of (**A**) Factor 2 (representing the coarser fraction of detritus) contribution to samples and volume percent of coarse fraction directly measured in selected samples (Tada et al., Chap. 25, this volume), (**B**) Factors 1 and 3 (representing the finer fraction of detritus from felsic and mafic sources, respectively) contribution to samples, and (**C**) the estimated mafic contribution to the finer grained fraction calculated as Factor 3/(Factor 1 + Factor 3). Sand layers and patches based on visual core description and observation on X-ray radiographs by Tada et al. (Chap. 25, this volume) are indicated by the shaded bands in the profiles. The marine isotope stage (MIS) boundary (top panel) is based on Kennett et al. (Chap. 21, this volume).

hanced delivery to Site 1017 during MIS 2 of detritus derived from north-central California.

ACKNOWLEDGMENTS

We express our special thanks to Drs. I. Koizumi and R. Tada for their encouragement and support throughout the course of this study. We are grateful to S.E. Calvert for giving us generous access to his XRF instrumentation. We would also like to express our sincere thanks to all the participants and shipboard staff of ODP Leg 167, and the staff at the ODP Gulf Coast Repository for help with the sampling. Thanks also go to Dr. R. Behl for discussion, and to Messrs. S. Sato and H. Matsui at the University of Tokyo, and K. Gordon and M. Soon at U.B.C. for their assistance in the laboratory. T. Irino is a Research Fellow of the Japan Society for the Promotion of Science. This research is supported by the Grant-in-Aid for Scientific Research of the Ministry of Education, Science and Culture of Japan No. 8-1425 and the Natural Sciences and Engineering Research Council of Canada.

REFERENCES

Behl, R.J., and Kennett, J.P., 1996. Brief interstadial events in the Santa Barbara Basin, NE Pacific, during the last 60 kyr. *Nature,* 379:243–246.

Benson, L., Kashgarian, M., and Rubin, M., 1995. Carbonate deposition, Pyramid Lake subbasin, Nevada: 2. Lake levels and polar jet stream positions reconstructed from radiocarbon ages and elevations of carbonates (tufas) deposited in the Lahontan basin. *Palaeogeogr., Palaeoclimatol., Palaeoecol.,* 117:1–30.

Calvert, S.E., Cousens, B.L., and Soon, M.Y.S., 1985. An X-ray fluorescence spectrometric method for the determination of major and minor elements in ferromanganese nodules. *Chem. Geol.,* 51:9–18.

Calvert, S.E., and Pedersen, T.F., 1993. Geochemistry of Recent oxic and anoxic marine sediments: implications for the geological record. *Mar. Geol.,* 113:67–88.

Crusius, J., Calvert, S., Pedersen, T., and Sage, D., 1996. Rhenium and molybdenium enrichments in sediments as indicators of oxic, suboxic and sulfidic conditions of deposition. *Earth Planet. Sci. Lett.,* 145:65–78.

Cullers R.L., 1994. The controls on the major and trace element variation of shales, siltstones, and sandstones of Pennsylvanian-Permian age from uplifted continental blocks in Colorado to platform sediment in Kansas, USA. *Geochim. Cosmochim. Acta,* 58:4955–4972.

Dansgaard, W., Johnsen, S.J., Clausen, H.B., Dahl-Jensen, D., Gundestrup, N.S., Hammer, C.U., Hvidberg, C.S., Steffensen, J.P., Sveinbjörnsdottir, A.E., Jouzel, J., and Bond, G., 1993. Evidence for general instability of past climate from a 250-kyr ice-core record. *Nature,* 364:218–220.

Dean, W.E., and Gardner, J.V., 1998. Pleistocene to Holocene contrasts in organic matter production and preservation on the California continental margin. *GSA Bull.,* 110:888–899.

Dean, W.E., Gardner, J.V., and Piper, D.Z., 1997. Inorganic geochemical indicators of glacial-interglacial changes in productivity and anoxia on the California continental margin. *Geochim. Cosmochim. Acta,* 61:4507–4518.

Doose, H., Prahl, F.G., and Lyle, M.W., 1997. Biomarker temperature estimates for modern and last glacial surface waters of the California Current system between 33° and 42°N. *Paleoceanography,* 12:615–622.

Ganeshram, R.S., and Pedersen, T.F., 1998. Glacial-interglacial variability in upwelling off NW Mexico: implications for Quaternary palaeoclimate. *Paleoceanography,* 13:634–645.

Gardner, J.V., Dean, W.E., and Dartnell, P., 1997. Biogenic sedimentation beneath the California Current system for the past 30 kyr and its paleoceanographic significance. *Paleoceanography,* 12:207–225.

Graham, D.W., Bender, M.L., Williams, D.F., and Keigwin, L.D., Jr., 1982. Strontium-calcium ratios in Cenozoic planktonic foraminifera. *Geochim. Cosmochim. Acta,* 46:1281–1292.

Horne, R.A., 1969. *Marine Chemistry: the Structure of Water and the Chemistry of the Hydrosphere:* New York (Wiley & Sons).

Kutzbach, J.E., Guetter, P.J., Behling, P., and Selin, R., 1993. Simulated climatic changes: results of the COHMAP climate-model experiments. *In* Wright, HE. Jr., Kutzbach, J.E., Webb, T., III., Ruddiman, W.F., Street-Perrott, F.A., Bartlein, P.J. (Eds.), *Global Climates since the last Glacial Maximum:* Minneapolis (Univ. Minn. Press), 24–94.

Lyle, M., Koizumi, I., Richter, C., et al., 1997. *Proc. ODP, Init. Repts.,* 167: College Station, TX (Ocean Drilling Program).

Lyle, M., Zahn, R., Prahl, F., Dymond, J., Collier, R., Pisias, N., and Suess, E., 1992. Paleoproductivity and carbon burial across the California Current: the Multitracers Transect, 42°N. *Paleoceanography,* 7:251–272.

Matsuo, S., 1989. *Geochemistry:* Tokyo (Kodansha). (In Japanese)

Miesch, A.T., 1976. Q-mode factor analysis of geochemical and petrologic data matrices with constant row-sums. *Geol. Surv. Prof. Pap. U.S.,* 574–G:1–47.

Mortyn, P., Thunell, R., Anderson, D., Stott, L., and Le, J., 1996. Sea surface temperature changes in the Southern California Borderlands during the last glacial-interglacial cycle. *Paleoceanography,* 11:415–430.

Norris, R.M., and Webb, R.W., 1990. *Geology of California* (2nd Ed.): New York (Wiley & Sons).

Piper, D.Z., 1994. Seawater as the source of minor elements in black shales, phosphorites and other sedimentary rocks. *Chem. Geol.,* 114:95–114.

Strickland, J.D.H., and Parsons, T.R., 1972. *A Practical Handbook of Seawater Analysis:* Ottawa (Fisheries Research Board of Canada).

Taylor, S.R., and McLennan, S.M., 1985. *The Continental Crust: Its Composition and Evolution:* Oxford (Blackwell Scientific).

Thomson, J., Jarvis, I., Green, D.R.H., Green, D.A., and Clayton, T., 1998. Mobility and immobility of redox-sensitive elements in deep-sea turbidites during shallow burial. *Geochim. Cosmochim. Acta,* 62:643–656.

Trask, P.D., 1952. Source of beach sand at Santa Barbara, California as indicated by mineral grain studies. *Univ. Calif. Tech. Rep. Eng.,* Ser. 14, no. 11.

Wilson, M., 1989. *Igneous Petrogenesis: A Global Tectonic Approach:* London (Unwin Hyman).

Date of initial receipt: 21 October 1998
Date of acceptance: 10 May 1999
Ms 167SR-209